Journal of Geophysical Research: Oceans

RESEARCH ARTICLE
10.1029/2017JC013602

Agulhas Current Meanders Facilitate Shelf-Slope Exchange on the Eastern Agulhas Bank

Neil Malan[1,2,3], **Bjorn Backeberg**[3,4,5], **Arne Biastoch**[6], **Jonathan V. Durgadoo**[6], **Annette Samuelsen**[5], **Chris Reason**[2], **and Juliet Hermes**[1,2,7]

[1]SAEON Egagasini Node, Cape Town, South Africa, [2]Department of Oceanography, University of Cape Town, Cape Town, South Africa, [3]Nansen-Tutu Centre for Marine Environmental Research, University of Cape Town, Cape Town, South Africa, [4]Coastal Systems, Natural Resources and the Environment, Council for Scientific and Industrial Research, Stellenbosch, South Africa, [5]Nansen Environmental and Remote Sensing Center, Bergen, Norway, [6]GEOMAR Helmholtz Centre for Ocean Research Kiel, Kiel, Germany, [7]Nelson Mandela University, Port Elizabeth, South Africa

Key Points:
- Agulhas Current meanders drive upwelling events and have an influence on shelf-slope exchange
- Large meander events are associated with warm intrusions at the shelf edge and cooling at depth
- Changes in bathymetry cause different meander-driven upwelling regimes along the Agulhas Current

Correspondence to:
N. Malan,
neilcmalan@gmail.com

Citation:
Malan, N., Backeberg, B., Biastoch, A., Durgadoo, J. V., Samuelsen, A., Reason, C., & Hermes, J. (2018). Agulhas Current meanders facilitate shelf-slope exchange on the Eastern Agulhas Bank. *Journal Geophysical Research: Oceans*, *123*. https://doi.org/10.1029/2017JC013602

Received 31 OCT 2017
Accepted 25 MAY 2018
Accepted article online 8 JUN 2018

Abstract Large solitary meanders are arguably the dominant mode of variability in the Agulhas Current. Observational studies have shown that these large meanders are associated with strong upwelling velocities and affect the shelf circulation for over 100 days per year. Here 10-year time series from two ocean general circulation models are used to create a composite picture of the Agulhas Current and its interactions with the shelf circulation in meandering and nonmeandering modes. Both models show good agreement with the size, propagation speed, and frequency of observed meanders. These composite meanders are then used to examine the response of shelf waters to the onset of large meanders, with the use of model output enabling the dynamics at depth to be explored. Results show a composite mean warming of up to 3°C of depth-averaged temperature along the shelf edge associated with an intrusion of the current jet onto the shelf driven by an intensification of the flow along the leading edge of large meanders. However, this intensification of flow results in cooling of bottom waters, driving cold events at the shelf break of <10°C at 100 m. Thus, the intensification of the current jet associated with large meander events appears to drive strong up and downwelling events across the inshore front of the Agulhas Current, facilitating shelf-slope exchange.

Plain Language Summary Agulhas Current meanders are some of the largest events that take place in the Agulhas Current system. They have a large impact on the shelf circulation and are important for the life cycle of several marine species. Here two ocean models, as well as satellite observations, are used to examine how meander events change the way in which the Agulhas Current interacts with the continental shelf of southeast Africa. It is found that meanders influence the pathways by which water is upwelled from below the Agulhas Current up onto the shelf, thus influencing the supply of nutrients to the shelf ecosystem.

1. Introduction

Large solitary meanders, commonly referred to as Natal Pulses, are a well-documented feature of the otherwise stable flow of the northern Agulhas Current (Lutjeharms, 2006; Lutjeharms & Roberts, 1988). They manifest as large offshore meanders of the Agulhas Current, with an associated cyclonic circulation and cold water core inshore of the meander. These large solitary meander events do not have a discernible seasonal cycle but display considerable interannual variability (Krug & Tournadre, 2012). Events occur an average of 1.6 times per year (Rouault & Penven, 2011), and although up to six events per year have been observed (de Ruijter et al., 1999), periods of 2 years without a large meander event have also been documented (Beal et al., 2015). These large solitary meanders, mostly originating north of 30°S, grow as they propagate downstream at a speed of 15–20 km per day (Lutjeharms, 2006).

Work on Natal Pulses has focused mainly on their frequency and generation mechanism (de Ruijter et al., 1999; Lutjeharms & Roberts, 1988; Tsugawa & Hasumi, 2010), as well as their possible impact as an upstream control on Agulhas Ring shedding and thus interocean exchange via the Agulhas Leakage (de Ruijter et al., 1999; Lutjeharms et al., 2003; Schouten et al., 2002; van Leeuwen et al., 2000). However, moored and satellite

observations point toward this link being less robust than previously thought (Elipot & Beal, 2015; Rouault & Penven, 2011).

Recent work has begun to focus on the regional impacts of Natal Pulses. Krug et al. (2014) used a combination of along-track altimetry and in situ mooring data in the southern Agulhas Current to show Natal Pulses as a major driver of variability along the eastern edge of the Agulhas Bank, influencing the circulation for an estimated 110 days a year. Further north, at 33.5°S, Leber and Beal (2015) examined the role of Natal Pulses on water mass modification via meander-induced upwelling, finding that meanders drive upwelling velocities of at least 13 m/day. A second study (Leber et al., 2016) at 33.5°S showed that upwelling events, driven by a combination of Agulhas Current and wind-driven upwelling, can raise central waters more than 130 m upward onto the shelf, resulting in cooling of up to 9°C at 50 m and a surface expression of cooling greater than 4°C.

The formation of large meanders was originally suggested to be due to barotropic instability in the Agulhas Current caused by the steep topography anomaly where the shelf widens at the Natal Bight (hence the term *Natal Pulse*), triggering perturbations that grow and propagate as large offshore anticyclones down the Agulhas Current (de Ruijter et al., 1999). Later work using a ocean general circulation model, and removing the effect of the Natal Bight topography, showed that the topography was not necessary to trigger large meander events, with meanders rather being generated by the interaction of the mean flow of the Agulhas Current with large anticyclonic eddies propagating toward the current from the upstream regions of the Mozambique Channel and from south of Madagascar (Tsugawa & Hasumi, 2010). The interaction of these anticyclonic eddies with the high potential vorticity (PV) gradient, which exists along the coast causes the inshore cyclone associated with large meander events to grow through a vortex stretching mechanism demonstrated by the numerical simulations of Tsugawa and Hasumi (2010). Elipot and Beal (2015) present the first detailed examination of the vertical structure of large meanders, using a full-depth array of current meter moorings. A new rotary empirical orthogonal function technique was used to highlight large meanders as the dominant mode of variance in the Agulhas Current while also separating out the influence of the smaller meander modes.

However, much of the shelf area inshore of the Agulhas Current lies south of 34°S where the Eastern Agulhas Bank introduces a broadening of the shelf. This area is important to the spawning of several fish and invertebrate species, several of them commercially important (Hutchings et al., 2002) and with the shelf circulation, especially the influence of the Agulhas Current in upwelling and advecting nutrients onto the shelf, as an important driver of their life cycles (Roberts, 2005; Roberts et al., 2010).

Modeling work on the Agulhas Undercurrent (Biastoch et al., 2009) suggests that large meander events are capable of causing the undercurrent to increase in strength and intrude up the shelf break, where it becomes indiscernible from the eastward countercurrent inshore of the Agulhas Current (described in Lutjeharms, 2006, and recently by Krug et al., 2017). However, little is known about the links between this deep upwelling and higher-frequency upwelling processes on the shelf.

Shelf edge upwelling is present inshore of all the major western boundary currents (Condie, 1995; Gill & Schumann, 1979; Roughan, 2004) and is primarily forced by interactions of the western boundary current with the bathymetry. In the Agulhas System south of 32°S, there is an area of semipermanent upwelling on the extreme eastern edge of the Agulhas Bank along the narrow shelf between 26°E and 28°E (Lutjeharms et al., 2000). The role of Ekman veering in the bottom layers as a strong driver of upwelling and shelf-slope exchange has been examined in detail in the East Australian Current (Roughan, 2004; Roughan & Middleton, 2002; Schaeffer et al., 2013), but this process has not been observed directly in the Agulhas Current system and its significance as an upwelling mechanism is yet to be quantified.

The relationship of the shelf circulation with Natal Pulses and other meander events in this area of broadening shelf is further complicated by the bimodal nature of the Agulhas Current's stability as the shelf broadens and shallows south of 34°S (Speich et al., 2006). Here in what is called the southern Agulhas Current, the core of the flow lies within nine tenths of the internal radius of deformation (approximately 30 km; Chelton et al., 1998) from the shelf break (i.e., 27 km offshore of the shelf break), compared to the distance of one tenth of the deformation radius in the northern Agulhas Current (i.e., 3 km offshore of the shelf break). Analysis of the effect of this change in the shelf-slope configuration on the Agulhas' path using a two-layer, linear stability model showed that the theoretical instability of the southern Agulhas is twice that of the instability

of the northern Agulhas (Paldor & Lutjeharms, 2009). In this complex dynamical environment, the origin of the bottom water of the Agulhas Bank shelf waters is still an open question. Observational studies using water masses to explore the origin of Agulhas Bank bottom water and the associated thermocline structure (Chapman & Largier, 1989; Largier & Swart, 1987; Swart & Largier, 1987) find a continuous, strong thermocline, which deepens toward the west, making the majority of the shelf waters south of 34°S a two-layer system. It was suggested by Largier and Swart (1987) that the deepening of the thermocline to the west was a result of the thermocline to the east being advectively controlled by the Agulhas Current, while the thermocline to the west is maintained by a combination of wind-driven coastal upwelling and advection of warmer water from the east. A result of this is that the seasonality increases in the western part of the Agulhas Bank.

Here we look at large meanders in the Agulhas through the lens of their direct and indirect effects in forcing the circulation over the shelf regions inshore of the main current jet, as well as examining their role in setting up the temperature and thermocline structure over the Agulhas Bank. The use of ocean models rather than the sparse observational data available enables subsurface, current-driven upwelling dynamics to be examined within a simpler, more spatially and temporally consistent framework in order to explore the upwelling mechanisms identified in previous observational studies. The aim is to examine these dynamics in a way that places past and future observations into context. As a dominant mode of variability along the inshore edge of the Agulhas Current, it is important that we understand the impacts and spatiotemporal variability of large meander events on the shelf waters of southern Africa.

2. Methods

2.1. Model Configurations

In this study, output from two different ocean general circulation models is analyzed. The goal of this multimodel approach is to supply a more robust analysis as numerical models in the Agulhas Current are prone to systematic biases and diverging solutions (Penven et al., 2011) dependent on choice of vertical coordinate, numerics (Backeberg et al., 2009; Barnier et al., 2006), lateral boundary conditions and resolution (Quartly et al., 2013). It must be emphasized that this is by no means a direct intermodel comparison; the two models used are different in terms of model code, forcing products, coordinate system, and bathymetry, although both are nested regional models at the same resolution of 1/10°. Both INALT01 (Biastoch et al., 2015; Cronin et al., 2013; Durgadoo et al., 2013; Le Bars et al., 2014; Loveday et al., 2014) and AGU-HYCOM (Hybrid Coordinate Ocean Model; Backeberg et al., 2009, 2014; Backeberg & Reason, 2010; Halo et al., 2014; Holton et al., 2017) configurations have been evaluated and proven fit for purpose in multiple publications on the dynamics of the greater Agulhas Current region.

AGU-HYCOM (Backeberg et al., 2014) is a southern African regional configuration of the HYCOM (Bleck, 2002), with a domain of 10°–50°S, 0°–60°E, nested inside a basin-scale HYCOM of the Indian and Southern Oceans (George et al., 2010). The inner AGU-HYCOM nest received snapshot boundary conditions from the parent model every 6 hr in a one-way nesting approach. Slowly changing variables are relaxed toward the outer model with a buffer zone of 20 grid cells, while the higher-frequency barotropic velocities and pressure fields are initialized using the bounded derivative approach of Browning and Kreiss (1982). AGU-HYCOM has 30 hybrid vertical layers, which transition smoothly from isopycnal coordinates in the ocean's interior to fixed z level coordinates in the surface mixed layer and shallow coastal areas. Lateral momentum boundary conditions are no slip. Bathymetry is interpolated onto the model grid from the 1-min resolution General Bathymetric Chart of the Oceans.

AGU-HYCOM is forced with 6-hourly fields from ERA-interim reanalysis (Dee et al., 2011), interpolated onto the model grid from its original 0.7° × 0.7° resolution. Monthly estimates of river discharge from the TRIP05 (Oki & Sud, 1998) hydrological model, using runoff from from ERA-interim, are also included and treated as a negative salinity flux with additional mass exchange (Schiller & Kourafalou, 2010).

INALT01 is a high-resolution nest within a global coarse-resolution ocean/sea ice configuration (Durgadoo et al., 2013), based on the Nucleus for European Modelling of the Ocean (Madec, 2008). The 1/10° domain is 8°N–50°S, 70°W–70°E, two-way nested into the global 1/2° grid using a two-way nesting approach (Debreu & Blayo, 2008). There are 46 vertical layers in z coordinates, 10 of which are in the top 100 m, and the deepest grid box is allowed to be partially filled (Barnier et al., 2006). Lateral momentum boundary conditions are free slip. Bathymetry from the 2-min resolution Gridded Global Relief Data (ETOPO2v2), is interpolated onto the nested model grid.

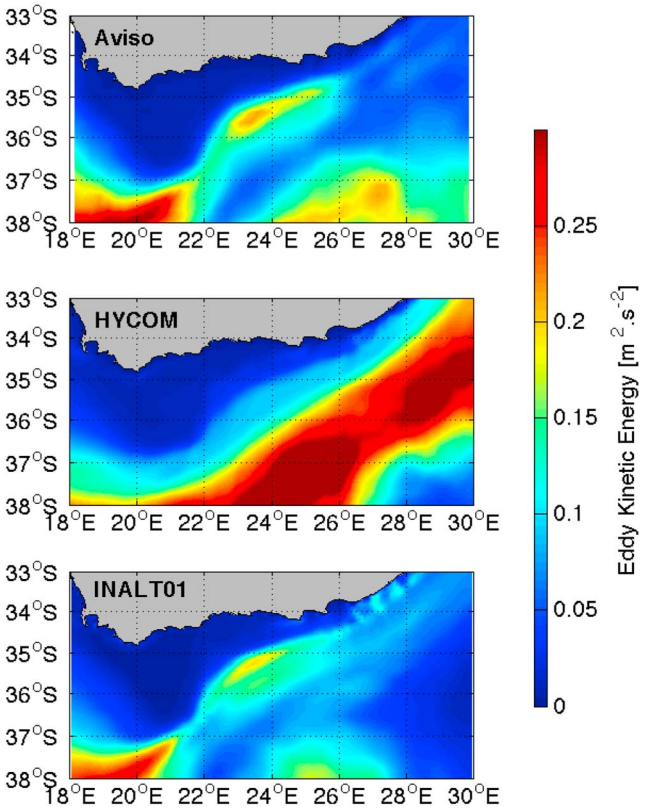

Figure 1. Climatology of annual mean eddy kinetic energy from 1997 to 2008. HYCOM = Hybrid Coordinate Ocean Model.

INALT01 is forced using COREv2b (Large et al., 1994) atmospheric and flux fields interpolated onto the model grid from its original 2° × 2° resolution. Neither model includes tides. A common time period of daily output for both models from 1997 to 2008 is used in this study. The differing model setups and forcing result in two alternate model representations of the Agulhas Current, which often fall on either side of observation. An example of this is shown in Figure 1: AGU-HYCOM shows high eddy kinetic energy (EKE) values offshore of the Agulhas Current when compared to AVISO's Allsat merged geostrophic velocities, while INALT shows far better agreement to the satellite-derived EKE. (A more in depth analysis of the reasons for this EKE bias in HYCOM can be found in Backeberg et al., 2014.) Results from one model are checked against that of the other model, and processes represented in both models are considered to be more robust and less likely to be caused by model artifact.

2.2. Large Meander Identification

The method for identifying meanders in the Agulhas Current is based on a technique used in previous studies of satellite observations at satellite ground track 020 (Krug & Tournadre, 2012; Rouault & Penven, 2011), where geostrophic velocities calculated from the merged MADT (http://www.aviso.altimetry.fr/duacs/), with a 1/3° resolution and daily output based on 7-day moving averages were interpolated onto satellite ground track 020 at a 0.1° resolution. The core of the Agulhas Current was selected as the position of the local maxima of alongshore flow. Use of gridded altimetry was found to be as effective as along-track altimetry for the identification of large meanders using this method (Krug & Tournadre, 2012). Due to the greater coherence in time of model data in comparison to the observations, the model output does not have to be filtered in space or time, as is done in studies using satellite altimetry. Instead, the position of the first peak of sea surface height gradient is used to reduce the noise from the daily velocity fields. This allows the higher-frequency dynamics of the shelf circulation to be more thoroughly investigated at a daily timescale.

To identify meanders, a transect along satellite ground track 020 (Figure 2) is extracted from the model. The location of this section is chosen for two reasons: first, its location at a key dynamic point in the Agulhas Current, where the shelf begins to widen onto the Agulhas Bank, and second, to remain consistent with earlier work and enable comparisons with observational studies.

Along this transect the surface current speed is calculated and local maxima in these speeds are identified (represented by the green dots in the right-hand panel of Figure 2). Surface speed is used rather than a velocity

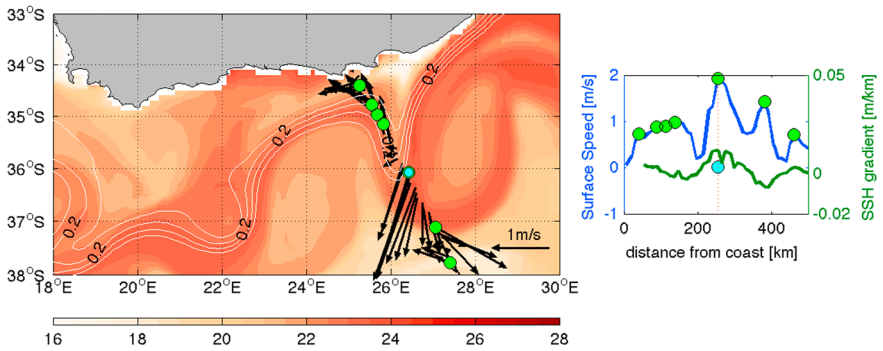

Figure 2. Snapshot of the technique used to identify the position of the Agulhas Current. In the main pane, sea surface temperature is shaded, selected contours of sea surface height (SSH) are shown in white, and velocity vectors along satellite track 020 are shown in black. Green dots show peaks in surface speed along track 020, while the blue dot shows the first peak in SSH gradient. In the right-hand panel, the surface speed and SSH gradient are plotted along track 020, with the vertical red line showing the position of the Agulhas Current.

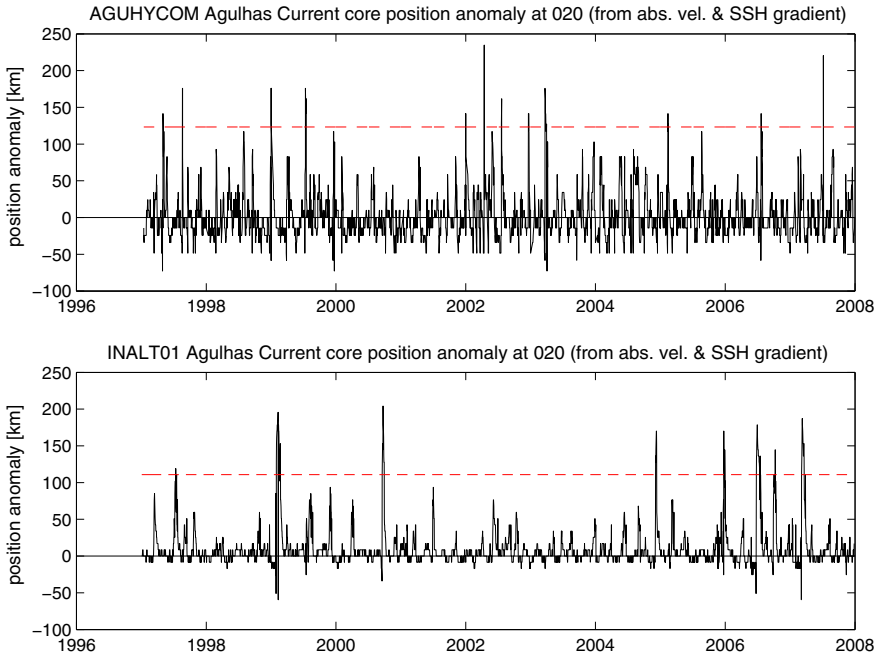

Figure 3. Time series of Agulhas Current position anomaly on ground track 020. Red dashed lines show 4 standard deviation threshold; AGU-HYCOM is shown in the top panel, and INALT01 in the bottom panel. SSH = sea surface height; HYCOM = Hybrid Coordinate Ocean Model.

vector so as to ensure that the changes in the current's direction as it meanders are not misinterpreted as decreases in along-current velocity. However, this leaves the problem of misidentifying intense anticyclonic eddies offshore of the main current jet as being the current core itself. Thus, the sea surface height gradient along the track 020 transect is also calculated and the core of the current is defined as the peak in surface speed closest to the first major peak in sea surface height gradient. Once the position of the Agulhas Current core has been established, a time series can be extracted in order to examine large meander activity. In order to study only the large meanders, a threshold of 4 standard deviations from the current's mean path was chosen as it found to best capture large meanders with strong offshore anticyclones. However, the results and production of composites were found to be robust down to a threshold of 2 standard deviations, with 4 standard deviations chosen as it provided a cleaner time series.

The resultant time series produced by applying this method to 10 years of daily AGU-HYCOM and INALT01 output shows the distance of the current core from its normal (modal) position at a daily resolution and is shown in Figure 3.

3. Results

3.1. Position of the Agulhas Current Core

The 10-year time series of Agulhas Current core position anomalies at track 020 for both INALT01 and AGU-HYCOM (Figure 3) are both characterized by variability on a variety of temporal scales. There is no discernible seasonal cycle in either model, and spectral analyses (not shown) reveal the dominant mode of variability taking place at 70–100 days in INALT01 and 50–120 days in AGU-HYCOM. Applying the same analysis to AVISO's allsat merged MADT product (www.aviso.altimetry.fr/en/data/products/sea-surface-height-products/global/madt-h-uv.html; not shown) indicates a dominant peak at 100 days and a smaller peak at 50 to 70 days. Thus, neither of the models nor the altimetry-derived time series show a strong seasonal cycle. It is clear in Figure 3 that there is more submeander-scale variability in the AGU-HYCOM time series and that there is no synchronicity in the timing of meander events in the two models, a not unexpected result due to the high levels of internal variability in the Agulhas Current.

Table 1 shows a summary of basic statistics of Agulhas Current core position at track 020. Statistics for the satellite altimetry are taken for the same period as the model runs from Rouault and Penven (2011). The modal current position, as well as the mean, is shown, as the mode is statistically the position where the Agulhas

Table 1
Summary of Basic Statistics Using the Agulhas Core Detection Technique at Ground Track 020

At track 020	AGU-HYCOM	INALT01	AVISO
Modal current position (km)	113.4	89.3	109.0
Mean current position (km)	114.8	94.0	113.0
Standard deviation (km)	31.0	27.1	35.5
Large meander events per year	1.9	1.5	1.6
Propagation speed (km/day)	17	16	15

Current is most often and so is a more robust estimate of the *normal* current position than the mean, which will be skewed by the large offshore deviations of the large solitary meanders. Thus from here on, anomalies in the Agulhas Current's position are calculated from the mode of the position time series, rather than the mean. The average propagation speed is calculated using both satellite track 020 and the next track downstream (track 198) with the average propagation speed being defined as the lag at which the maximum correlation occurs between the time series of Agulhas Current position at each track.

Both models show good agreement with the observed meanders. Bearing in mind the lower resolution of the satellite observations, differences of less than 30 km are not considered to be significant. AGU-HYCOM shows slightly stronger agreement with satellite observations, while the Agulhas Current in INALT01 lies closer inshore, with less variability resulting in a lower standard deviation. However, INALT01 is closer to the observed 1.6 pulses per year at 1.5, compared to the 1.9 pulses per year of AGU-HYCOM.

It is notable that the broadening trend observed upstream by Beal and Elipot (2016) is not evident in either of the model time series as an offshore movement of the current core. This could be either as a result of the models' inability to simulate this trend in the Agulhas Current or alternatively that the broadening signal is not evident in the more variable southern Agulhas Current where the model time series have been extracted, several hundred kilometres downstream of the measurements of Beal and Elipot (2016).

3.2. Meander Composites

In order to examine the effect of large meanders on shelf temperatures and circulation over the duration of the time series, the core identification method at track 020 was used to create a composite picture of the Agulhas Current during both pulse and nonpulse periods. The *pulse* composite consists of the days in AGU-HYCOM and in INALT01 where the Agulhas Current core is further than 4 standard deviations from its modal position. In the nonpulse composite, the pulse days are removed from the time series, resulting in a representation of the current where there are no large meander events. Using the mean of the entire time series, apart from the meander days, in the nonpulse composite, ensures that the composite anomalies presented below are not affected by smaller-scale features such as shear edge border eddies. A surface view of the resulting composites for both AGU-HYCOM and INALT01 can be seen in Figure 4.

The meander composite manifests as a large offshore anticyclone, drawing the current core offshore, with the leading and trailing edges, or *wings* of the meander before and after the peak encroaching on the shelf slightly more than in the no-pulse composite. It is noted that the Agulhas Current in INALT01 is narrower and stronger, with weaker offshore anticyclones associated with meander events. The model meander composites were also checked against composites using satellite observed geostrophic currents from AVISO and satellite sea surface temperature from the Group for High Resolution Sea Surface Temperature (CMC0.2deg- CMC-L4-GLOB-v2.0; Brasnett, 2008). The shape and geometry of the composite meanders was consistent with observed meander events. In the nonmeandering composites, AGU-HYCOM (Figure 4b) shows a broader mean current compared to the satellite observations (Figure 4f), while INALT01 shows good agreement in the nonmeandering state (Figure 4d).

To assess the effect of large meanders on the whole water column over the shelf, pulse composite anomalies of the AGU-HYCOM depth-averaged temperatures down to 200 m are plotted in Figure 5 with lags before, during, and after the passage of the peak of the composite pulse. Twenty days before the passage of a large meander (Figure 5a), upwelling is enhanced along the narrow shelf east of 26°E, with composite depth-averaged temperatures inshore of the current up to 2°C below the mean. Ten days later in the composite (Figure 5b), strong positive anomalies in depth-averaged temperature are observed in the offshore anticyclone at 29°E. Inshore of this, the negative anomaly and inshore cyclone has cooled further and is beginning to detach

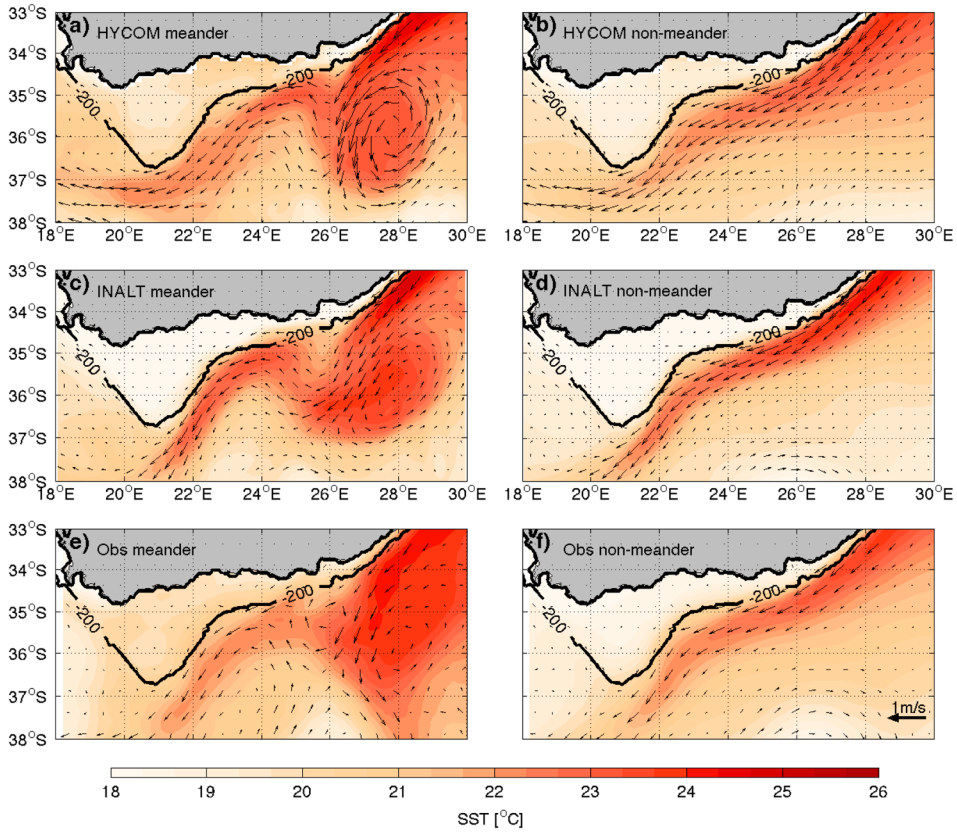

Figure 4. Mean AGU-HYCOM, INALT01, and satellite observed surface temperatures (°C) and surface current vectors for pulse composite (left column) and no-pulse composite (right column). (a) AGU-HYCOM meander composite, (b) AGU-HYCOM nonmeander composites, (c) INALT01 meander composite, (d) INALT01 nonmeander composite, (e) meander composite derived from AVISO geostrophic velocities and Group for High Resolution Sea Surface Temperatures, and (f) nonmeander composites from the same. HYCOM = Hybrid Coordinate Ocean Model; SST = sea surface temperature.

from the coastline as the shelf broadens to the east. When the peak of the pulse lies over track 020 (Figure 5c), a strong offshore anticyclone, with an associated 2°C warming anomaly is seen offshore centered at 28°E. Inshore of this anticyclone, the negative anomaly has weakened and moved further offshore, now flanking the north west side of the anticyclone. Inshore of this a zone of warm anomalies appears along the shelf edge between 24°E and 26°E. Ten days following the passage of the pulse across track 020 (Figure 5d), the offshore anticyclone has warmed further and moved offshore, now being centered on 37°S, 28°E. The cooling along the north west flank has further spread and dissipated, while the shelf edge warming first seen in the in Figure 5c has strengthened to up to 3°C and remains stationary at the shelf edge.

When the same pulse composite depth-averaged temperature anomalies are considered for INALT01 (Figure 6), similar patterns are observed. Key differences are in the strength of the cold inshore cyclone, which remains strong and coherent until 30 days after the passage of a meander (not shown), where it is advected offshore and dissipates, as it did on AGU-HYCOM at 10 days after meander passage. A similar pattern is seen when looking at the pulse composite anomalies of the surface relative vorticity normalized by the planetary vorticity.

$$\frac{\zeta}{f}$$

where

$$\zeta = \frac{dv}{dx} - \frac{du}{dy}. \tag{1}$$

The vorticity structure (Figure 7) at the area of widening shelf south of Port Elizabeth echoes the extended dipole structure seen in the depth averages temperatures (Figures 5 and 6). Of interest is that areas of strong

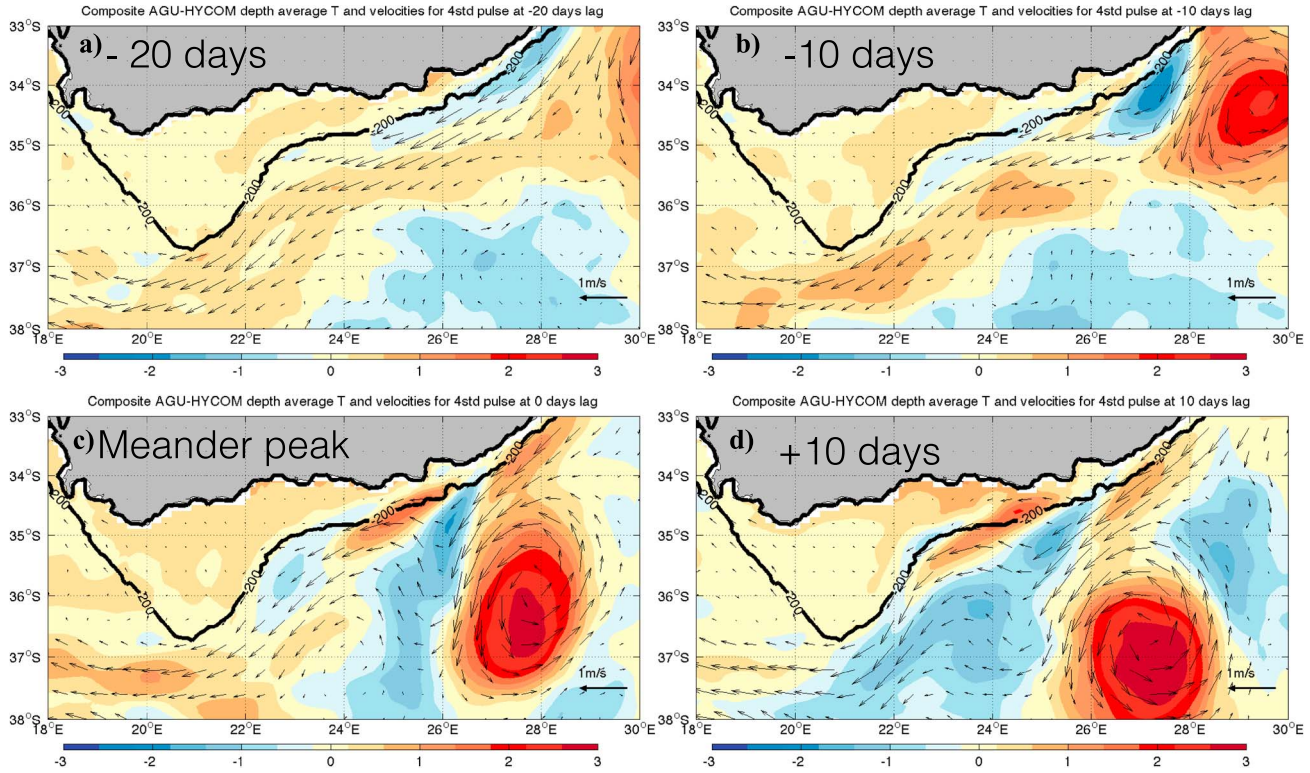

Figure 5. Depth-averaged AGU-HYCOM composite temperature anomalies (°C) in the top 200 m overlaid with composite surface currents (a) 20 days before, (c) 10 days before, (b) at peak passage, and (d) 10 days after the passage of the peak of a pulse over track 020. HYCOM = Hybrid Coordinate Ocean Model.

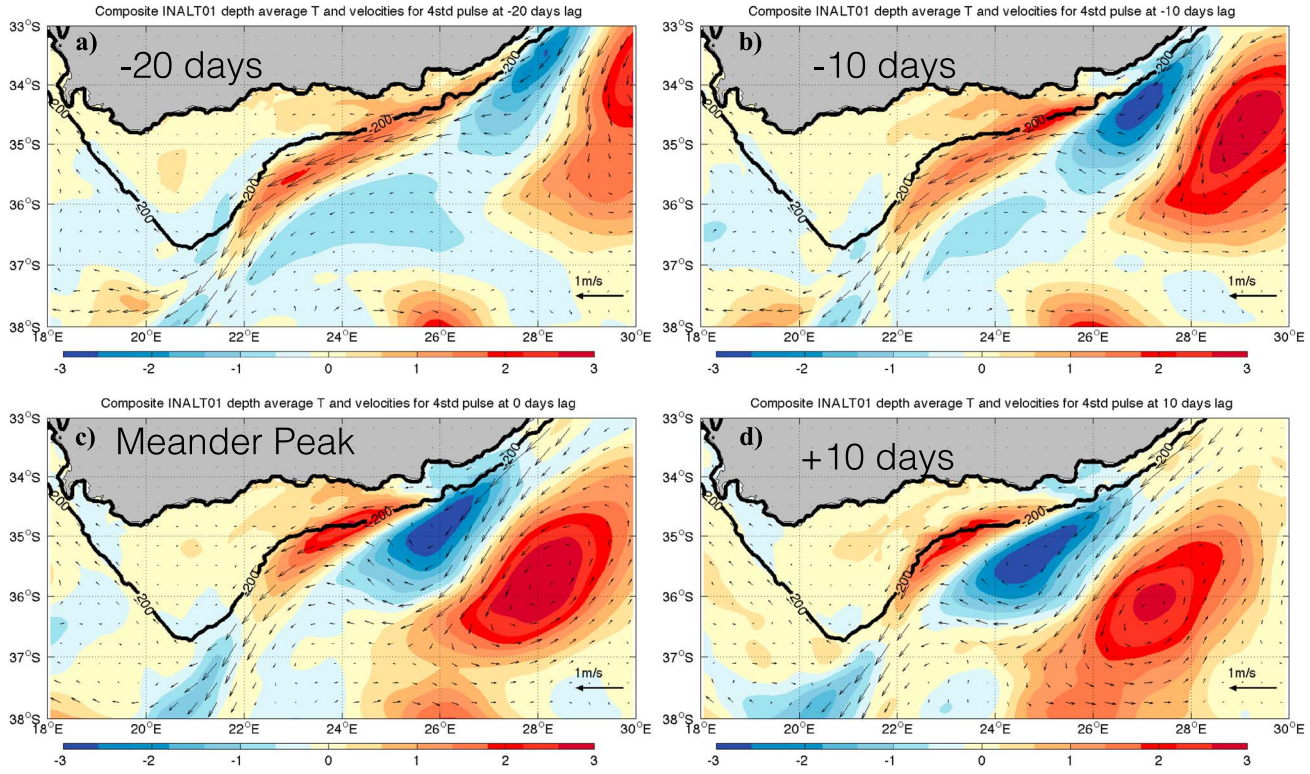

Figure 6. Depth-averaged INALT01 composite temperature anomalies (°C) in the top 200 m overlaid with composite surface currents (a) 20 days before, (c) 10 days before, (b) at peak passage, and (d) 10 days after the passage of the peak of a pulse over track 020.

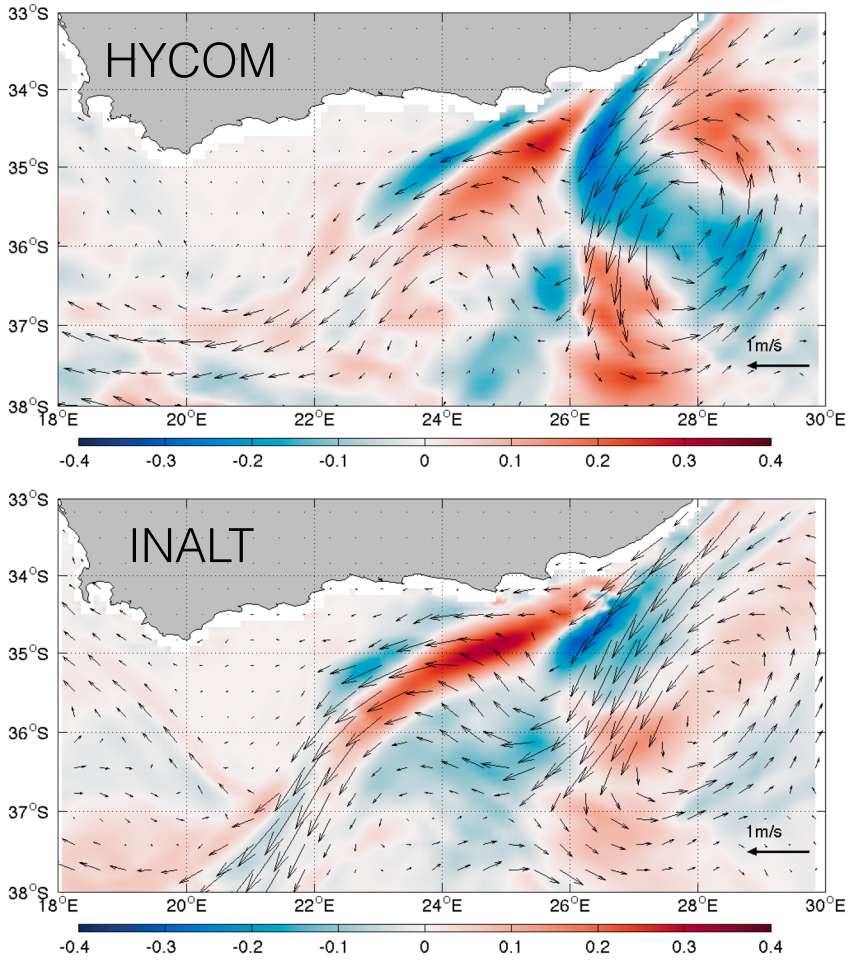

Figure 7. Pulse composite anomaly of normalized surface relative vorticity for AGU-HYCOM (top) and INALT01 (bottom) overlaid with pulse composite mean surface currents. HYCOM = Hybrid Coordinate Ocean Model.

cyclonic vorticity, inshore of the current from 26°E to 28°E, and along the shelf edge from 22.5°E to 24.5°E are associated with warm, rather than cold, temperature anomalies. This could suggest that vorticity dynamics at these scales are driven by shear at the inshore edge of the current, rather than the production of cyclonic eddies. Therefore, this cyclonic vorticity appears to be produced by warm Agulhas Current water being forced onto the shelf and strengthening the shear zone between the Current itself and the slower flowing shelf water. The intrusion of the Agulhas Current on the shelf edge in this shear zone can be seen in the warm temperature anomalies along the shelf edge downstream of Algoa Bay where the Agulhas Current Core begins to separate from the coast between 22°E and 26°E in Figure 6c.

3.3. Meander-Driven Cold Water Intrusions at the Shelf Edge

The meander composite anomalies above reveal that the shelf waters inshore of the Agulhas Current exhibit a slight (less than 1°C) and unexpected warming as a result of large meander events. However, this is not consistent with the strong links between large meander passage and upwelling reported in the observational literature. In order to investigate shelf-slope exchange during meander events more thoroughly, temperatures at 100-m depth along the shelf break are considered between 23°E and 26°E, where strong intrusion of warm surface water occurs (from here referred to as the EAB section, Figure 8). A year of the time series, from July 1998 to July 1999 is presented in the Hovmöller plots in the bottom panels of Figure 8. At 100-m depth, cold events propagate westward along the shelf edge, bringing cold anomalies of 3–4°C across the shelf break. There are approximately five of these cold intrusions per year, and they propagate faster and are longer lived than the warm events, where temperatures at 100 m can exceed 16°C.

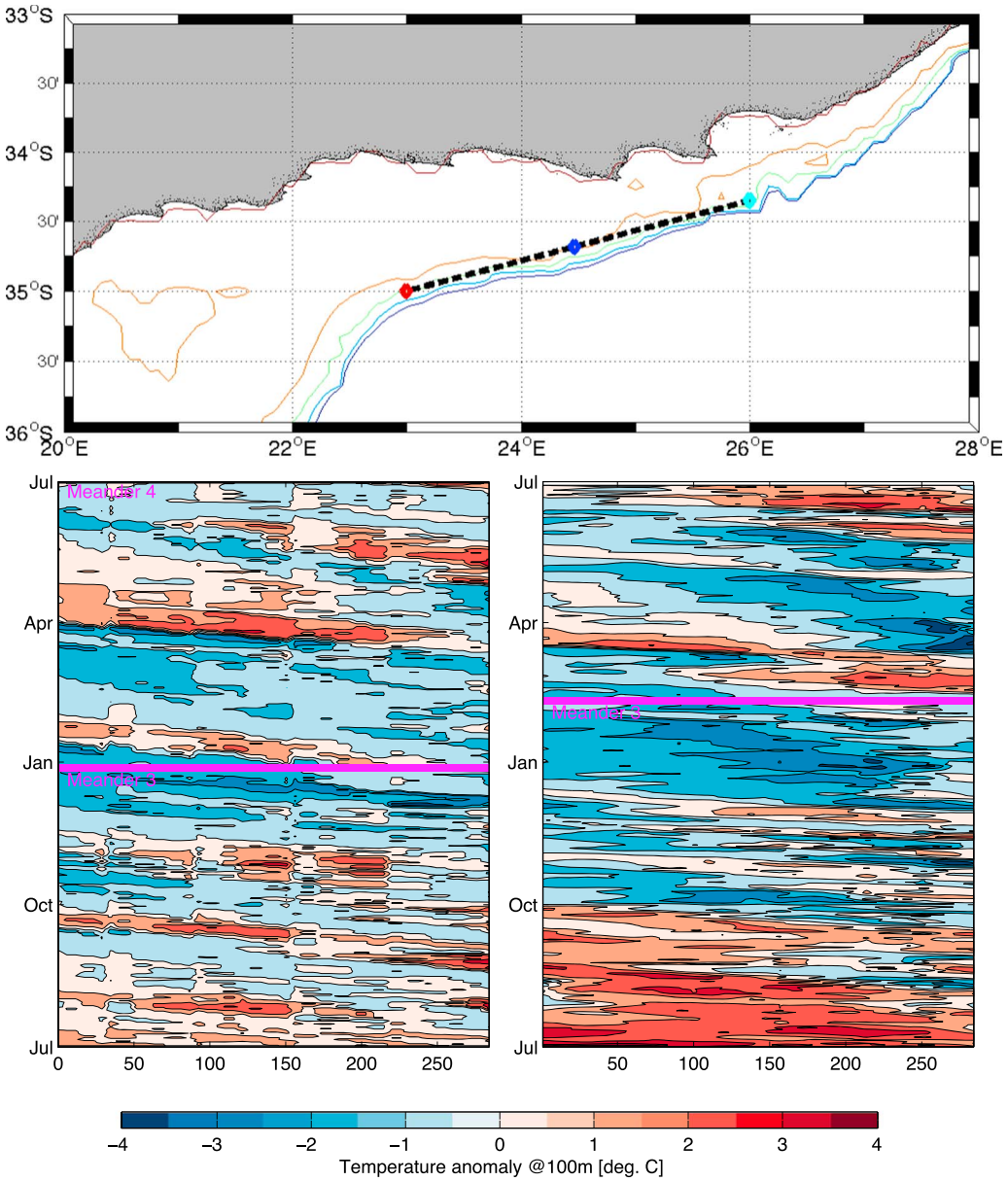

Figure 8. Hovmöller plot of temperature anomaly at 100 m along the shelf break from July 1998 to June 1999 in both AGU-HYCOM (left panel) and INALT01 (right panel), passage times of large meanders are indicated by horizontal lines. Location of the section is shown by the black dotted line in the top panel.

A series of lag correlations of temperature at 100 m at the beginning, middle, and end of this section (see colored markers in Figure 8), with the time series of Agulhas Current position anomalies presented in Figure 3 reveals the interesting pattern of the role large meander events play in driving temperature at depth on the shelf-edge (Figure 9). On the eastern edge of the EAB section, at 26°E, temperature at 100 m in INALT01 decreases 20 days before a positive anomaly in Agulhas Current position (i.e., a meander event) and then increases 10 days after the meander event. AGU-HYCOM shows a similar pattern of negative and then positive correlation, but with the strongest negative correlation at no lag and positive correlation 20 days after the meander. In the center of the section (24.5°E), INALT01 shows a slight, but significant, negative correlation 45 days before and 35 days after a meander and a strong positive correlation 2 days before a meander. AGU-HYCOM at 24.5°E shows a negative correlation 12 days before a meander and 6 days after a meander. Finally, at the western end of the section, while both models agree on a negative correlation

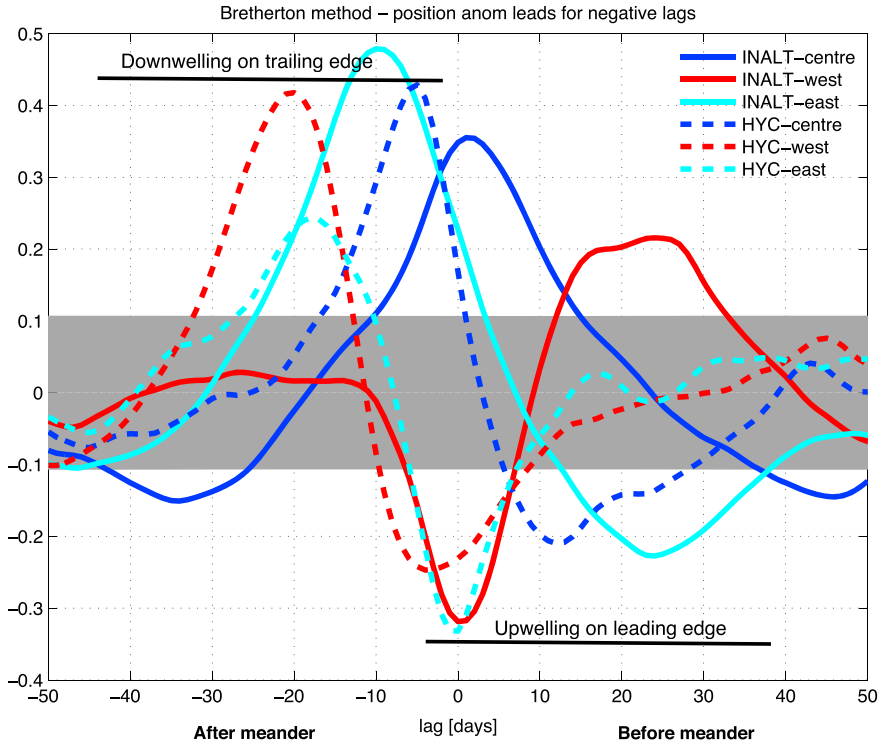

Figure 9. Lag correlation of Agulhas Current position at track 020 against temperature at 100 m along the 200-m isobath at start, middle, and end of 200-m isobath section. The 95% significance level is shaded in gray. AGU-HYCOM is shown in dashed lines, and INALT01 in solid lines. Colors represent location along Eastern Agulhas Bank section, with cyan being easternmost and red being westernmost. Positive (negative) lags represent a temperature response before (after) pulse passage.

between 5 and 0 days after a meander, INALT01 shows a strong positive correlation 15 to 25 days before a meander, while AGU-HYCOM shows a strong positive correlation 20 days after a meander.

Two things should be borne in mind when analyzing these lag correlations (Figure 9). First, as the Agulhas Current is strongly bounded by the bathymetry, negative anomalies in the current's position tend to be small compared to the large positive anomalies created by meanders. Thus, a negative correlation results in cooler temperatures, while a positive correlation results in warmer temperatures. Second, as the Agulhas Current position anomaly is only measured at track 020 (24.6°E), the different positions along the EAB section represent the response of the shelf edge temperatures at differing distances from the meander peak. Thus, a phase shift to the west (or *before meander*) is seen in the lags of the INALT01 output compared to AGU-HYCOM. This can be most clearly seen in the upwelling peaks in the center of the section (blue lines in Figure 9) where the positive correlation for INALT01 lags that of AGU-HYCOM by almost 10 days.

Thus, as a result of the slight difference in meander shape (see Figure 4), the upwelling and downwelling on the leading and trailing edge of the meander take place further west in INALT01 than in AGU-HYCOM, but the same pattern of upwelling associated with the leading edge of the meander, and downwelling associated with the passage and trailing edge of the meander is seen.

4. Discussion

4.1. Model Agreement

It is immediately apparent that AGU-HYCOM and INALT01 differ in terms of the amount of mesoscale variability, particularly in the form of anticyclonic eddies offshore of the Agulhas Current core. Despite this, both the meander composites produced by applying the current identification method, and the resulting temperature and vorticity structure in meandering and nonmeandering modes, show common dynamics. AGU-HYCOM does show meanders with a tighter loop (shorter wavelength and larger amplitude) than INALT01, due to the differing strength of these offshore anticyclones. While both models show good agreement in current core

position, variability, and meander geometry with observations (these comparisons can be skewed one way or the other by using a different metric of comparison, for example, Sea Surface Height rather than velocities, but are robust), the slightly shorter wavelength of meanders in AGU-HYCOM results in a stronger shear zone across the shelf break and temperature responses to meanders are at slightly different lead/lag times due to this difference in mean meander geometry between the two models.

However, the agreement in meander representation between two models with differing representation of the mean current (as seen in the EKE and mean current comparisons in Figures 1 and 4) points to the process of large meander formation being independent of model formulation and to some extent the state of the mean Agulhas Current. This supports the idea of large meanders being formed by nonlocal influences, as previously demonstrated by Tsugawa and Hasumi (2010).

4.2. Spatial Variability in Temperature During Meander Events

The meander composites reveal, to first order, that in both model simulations large meanders cause a small warming of the shelf waters to the west of 25°E. However, closer investigation shows a more complex interaction between the shelf waters, the shelf break, and the dynamic movement of the Agulhas Current caused by large solitary meanders. The depth-averaged temperatures presented in Figures 5 and 6 show that the cold temperature anomalies of the inshore cyclonic eddy associated with large meander events do not propagate down the coast further than Algoa Bay at 26°E, where the inshore cyclone instead begins to elongate, move offshore, and dissipate. Thus, the upwelling associated with this inshore cyclone is consistent with the large upwelling velocities measured at 33.5°S by Leber and Beal (2015) but does not seem to influence the wider Eastern Agulhas Bank south of 34°S. This breakdown of the structure of the inshore cyclone could be attributed to a decrease in depth and a relaxation in the shelf slope, as well as an increase in the amplitude of the meander (Paldor & Lutjeharms, 2009; Sutyrin, 2016). One way of understanding the erosion of the inshore cyclone within a meander could be in terms of conservation of PV where

$$\mathrm{PV} = \frac{\zeta + f}{h} \tag{2}$$

with ζ representing the relative vorticity of the inshore cyclone, f representing the planetary vorticity, and h representing the total water column depth at the location of the inshore cyclone. Initially, north of 34°S, where the shelf is narrow and steep, the inshore cyclone's center is offshore of the shelf break and h is relatively large. At this stage the cyclone is circular in shape and strongly expressed within the meander, with a defined negative temperature anomaly (see Figures 5b and 6b). As the meander then propagates downstream and encounters the widening and more relaxed shelf slope to the south of 34°S, the change in shelf configuration results in a decrease in h at the inshore edge of the cyclone. In order to conserve PV, in this situation where both PV and f are negative, ζ needs to become more positive. Figure 10 shows a schematic representation of this process. This input of anticyclonic relative vorticity can be seen in the plots of meander composite relative vorticity from both AGU-HYCOM and INALT01 in Figure 7 and manifests itself as a triangular area of positive relative vorticity extending downstream from 34°S, 26°E. This input of anticyclonic vorticity on the inshore edge of the the cyclone acts to erode it and move it offshore, toward the large offshore anticyclone, thus concentrating the core of the Agulhas Current, which is between the two. This process is consistent with observations from RAFOS floats by Pivan et al. (2016), who observed the inshore cyclone to lose coherence and move offshore as the shelf widened. The offshore movement and elongation of the inshore cyclone results in zones of convergence and divergence due to increased horizontal current shear immediately downstream of the meander. This produces the patterns of upwelling and downwelling during meander passage, shown by the correlations in Figure 9. It must be noted that this erosion of the inshore cyclone is delayed in INALT01 compared to AGU-HYCOM, occurring some 20 days later, a result of the longer wavelength of meander larger inshore cyclone and weaker offshore anticyclone than those observed in AGU-HYCOM.

4.3. Shelf Edge Upwelling

A robust result shown in the meander composites of both AGU-HYCOM and INALT01 is the presence of a zone of strong horizontal current shear extending between 22°E and 26°E. This strong shear between the shelf waters and fast-flowing water at the inshore edge of the current begins inshore of the 100-m isobath just west of Algoa Bay and extends diagonally offshore to 22°E. This shear causes strong cyclonic vorticity downstream of the meander as well as an intrusion of warm surface water, resulting in a composite warming anomaly of up to 3°C. This warm intrusion associated with meander passage has also been observed by Pivan et al. (2016) from satellite sea surface temperature in the form of a warm recirculating Agulhas plume. The warm anomalies

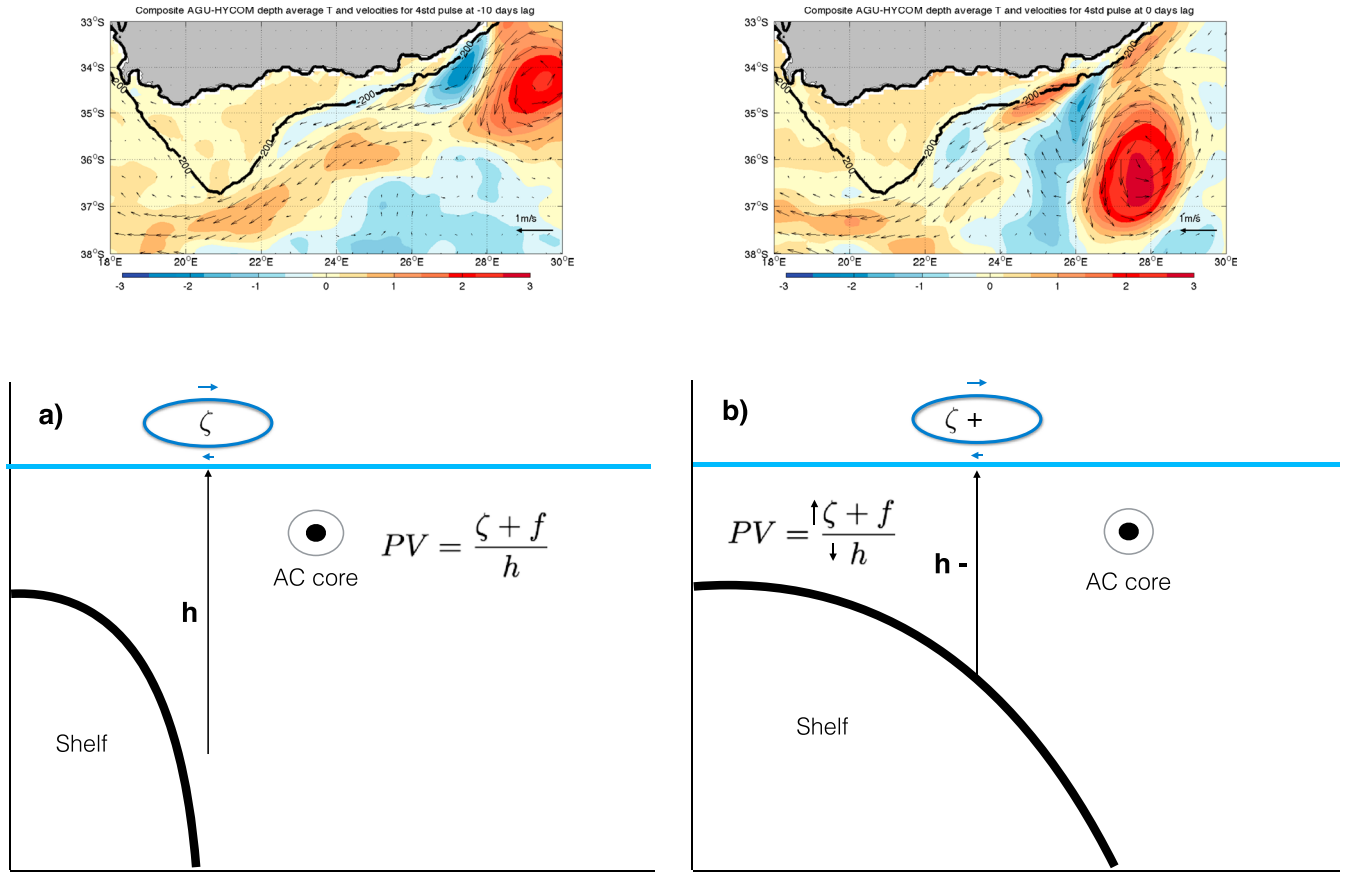

Figure 10. Schematic representation of the interaction between the cyclonic eddy inshore of a meander and the shelf. Upstream of 34°S where the shelf is steep and narrow and (b) downstream of 34°S where the shelf widens and acts to erode the inshore cyclonic eddy due to an increase in anticyclonic vorticity in the cyclone. The top panels (repeated from Figure 5) show the stages in meander passage represented by the schematic below.

in the depth-averaged temperature associated with these areas of strong cyclonic vorticity (Figures 5c and 6c) suggest that the core of the current interacts strongly with the calmer shelf waters, driving these shear processes. Thus, a case can be made that it is not the meander itself that is a strong driver of upwelling and shelf-slope exchange on the Eastern Agulhas Bank but rather the intensification of the interaction between the Agulhas Current's fast-flowing (>1 m/s) core with the shelf due to the effect of the meander *pushing* its leading edge onto the shelf. This produces a convergence of warm surface water at the shelf edge and an associated divergence, with upwelling and downwelling fronts as borne out by the temperature correlations during meander passage shown in Figure 9. The upwelling associated with this shear is then advected up and onto the shelf during the passage of the meander when shelf edge currents are strongest. The most likely process to drive this upwelling and advection associated with an intensification of the southwestward jet current with a shallowing topography would be Ekman veering in the bottom layer. This process has been considered in some detail during intensive observational studies in the East Australia Current (Roughan, 2004; Roughan & Middleton, 2002). From this work, if we consider the mass transport in the bottom boundary layer for a given alongshelf geostrophic current and bottom boundary layer thickness, they show that

$$w_c = \frac{\frac{1}{2} v_g \delta}{R_{oi}} \tag{3}$$

with w_c being the velocity at which water is lifted up the shelf, v_g the alongshore geostrophic current, δ the bottom boundary layer thickness, and R_{oi} being the internal Rossby radius. If we scale this for the Agulhas Shelf with an alongshore current of >1 m/s and estimated bottom boundary layer depth of 25 m (typical values from individual model sections) and an internal Rossby radius of 30 km, an uplift of water onto the shelf of 35 m per day is possible.

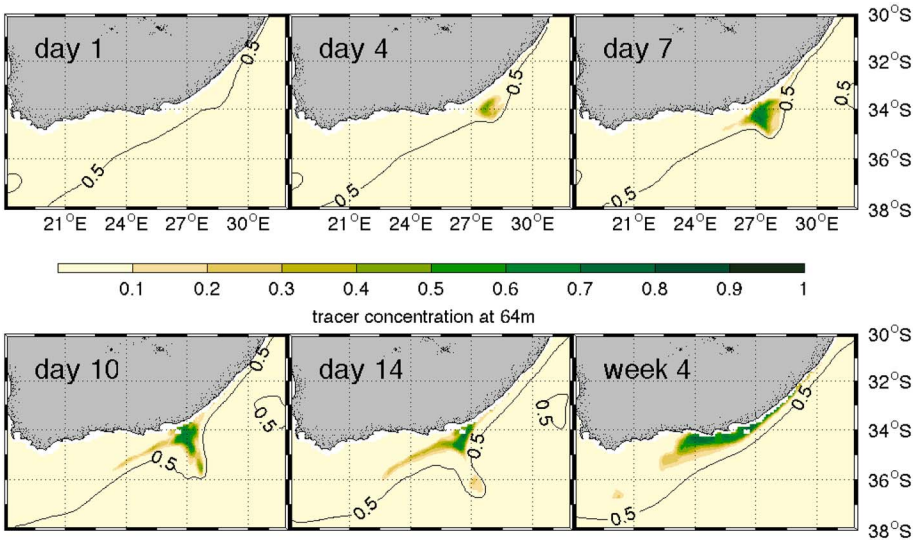

Figure 11. Tracer concentration at 64 m in AGU-HYCOM. Tracers were initialized below 400 m over a 6-week period during a meander event in 2001 and used as a proxy for upwelling. The 0.5-m sea level contour is highlighted to show the inshore edge of the current as the meander propagates along the coast.

However, it must be kept in mind that theoretical work has shown that, as this uplift occurs, buoyancy effects may become important (MacCready & Rhines, 1993) and lead to a shutdown of the bottom boundary layer at a timescale of days to a week. This shutdown time can be increased by an increase in bottom friction caused by an acceleration of the alongshore current (as observed in the East Australian Current by Roughan, 2004), and it is possible that this is the case during the passage of meanders in the Agulhas Current.

4.4. Case Study

To directly observe the uplift of water from beneath the Agulhas Current on the leading edge of a large meander and to test the knowledge gained from the composite analysis during a specific meander event, a tracer experiment was run using online tracers within the more variable of the two models, AGU-HYCOM. The tracers are initialized at a concentration of 1 below 400 m and 0 above 400 m. The model is then restarted and run for 6 weeks, with a meander passing track 020 2 weeks into the integration. Here we consider tracer concentration at a depth of 64 m to approximate the upwelling of nutrients in to the euphotic zone. Figure 11 shows daily averages of tracer concentration in the 2 weeks before the passage of a meander event. On day 4, the inshore cyclone of the meander becomes visible as an area of higher concentration at 28°E, 34°S. This then strengthens until day 7, whereafter (as in the composites above) it parks and begins to erode as it encounters the spreading of isobaths (Figure 11). This is seen on days 10 to 14, along with the formation of a thin strip of upwelling tracer extending southwest along the shelf edge. This is consistent with the Ekman bottom veering discussed above as the current intensifies and moves onshore at the leading edge of the meander. In the following weeks, this intrusion is advected onto the shelf and into the top 50 m of the water column and by week 4, upwelled tracer is widespread over the inner shelf. Although we do not see a cooling on the inner part of the shelf resulting from the passing of meanders, this experiment shows that the passing of a meander can potentially transport nutrients from deep water onto the inner part of the shelf, supporting primary production in the region. Strengthening the idea of Ekman veering being driven by an intensification of shelf edge flow, a correlation of shelf edge velocity anomalies with temperature, both near the bottom at 100 m, is performed (for the full 10-year time series of AGU-HYCOM, location marked in blue in the top panel of Figure 8). The results reveal a significant relationship ($r = 0.64$ at 99% confidence interval) with a drop in temperature lagging westward current anomalies by 1 day.

5. Conclusion

Two ocean models show, with small spatial differences, that large meander events drive strong shear between Agulhas Current core waters and shelf waters on their leading and trailing edges. This shear produces areas of strong negative vorticity and drives upwelling events in the bottom boundary layer, resulting in a significant decrease in subsurface temperatures at 100 m at the shelf edge. These areas of strong shear can move up

or down the shelf depending on the wavelength of the meander. The inshore cyclone associated with large meander events is advected offshore and eroded by the widening of the continental shelf west of 26°E and the relaxation of the shelf slope, thus creating a different upwelling regime in the shelf waters of the Agulhas Bank compared to the narrower shelf further upstream (north of 34°S).

Therefore, the supply of cold water from depth onto the Agulhas shelf is a byproduct of intensification of the flow during mesoscale meander events due to their interaction with a changing shelf slope, but the geographical location of this shelf edge upwelling will change with different meander geometry and thus may be sensitive to changes in the variability of the Agulhas Current. This is demonstrated by the temporally different upwelling responses seen in the two models used here. This shelf edge upwelling can be forced both by Ekman veering at the shelf edge, as well as a steepening of isotherms on the inshore edge of the current to maintain geostrophy in response to an intensification of the Agulhas Current core. Recent long-term observations (Beal & Elipot, 2016) indicate a broadening in the Agulhas Current as a result of increased EKE related to faster moving eddies noted in Backeberg et al. (2012). It is possible that this broadening could mean an eastward shift and intensification of shelf edge upwelling, as seen in AGU-HYCOM, which has a broader current and more mesoscale variability compared to the narrower, more stable Agulhas Current simulated by INALT01.

Interactions in the Eastern Agulhas Bank shear zone are complex and not sufficiently resolved in this study, with recent glider operations providing the first high-resolution observations of this front (Krug et al., 2017). This work revealed the generation of submesoscale cyclones as a result of shear instabilities during a nonmeandering phase of the current. The effect of the strengthening of the shear during meander events has on these frontal dynamics is currently not known and will require a new generation of submesoscale resolving ocean models to be examined in order to properly place these mechanisms into a larger context and fully understand the interactions of wind and current driving upwelling on the inner shelf.

Acknowledgments
The authors would like to thank two anonymous reviewers for their comments and input and Marjolaine Krug for providing her code for identifying Natal Pulses from altimetry data. AGU-HYCOM was run on Hexagon at the High Technological Centre in Bergen (project NS2993K), and raw data are archived on NIRD (www.sigma2.no) and are available upon request. INALT01 was developed at GEOMAR, with details of its configuration and access to raw data available at www.geomar.de/en/research/fb1/fb1-tm/ocean-models/inalt01/. Data and code for the reproduction of Figures 1- 9 and 11 can be found at https://github.com/nmalan/Agulhas_meanders. Altimetry data are available at www.aviso.altimetry.fr/en/data/products/sea-surface-height-products/global/madt-h-uv.html, and satellite SST data are available at podaac.jpl.nasa.gov/dataset/CMC0.2deg-CMC-L4-GLOB-v2.0. This work was funded by the the Professional Development Programme of the DST managed by the NRF-RISA, with additional funding through NRF grant 98183. The financial assistance of the NRF through SAEON toward this research is hereby acknowledged. Opinions expressed and conclusions arrived at are those of the authors and are not necessarily to be attributed to the NRF and SAEON. Additional funding from the German Federal Ministry for Education and Research (BMBF) framework project SPACES (03G0835A) and the Nansen Tutu Centre is also acknowledged.

References

Backeberg, B. C., Bertino, L., & Johannessen, J. A. (2009). Evaluating two numerical advection schemes in HYCOM for eddy-resolving modelling of the Agulhas Current. *Ocean Science*, *6*, 429–475. https://doi.org/10.5194/osd-6-429-2009

Backeberg, B. C., Counillon, F., Johannessen, J. A., & Pujol, M.-I. (2014). Assimilating along-track SLA data using the EnOI in an eddy resolving model of the Agulhas system. *Ocean Dynamics*, 1121–1136. https://doi.org/10.1007/s10236-014-0717-6

Backeberg, B. C., Penven, P., & Rouault, M. (2012). Impact of intensified Indian Ocean winds on mesoscale variability in the Agulhas system. *Nature Climate Change*, *2*(8), 608–612. https://doi.org/10.1038/nclimate1587

Backeberg, B. C., & Reason, C. J. C. (2010). A connection between the South Equatorial Current north of Madagascar and Mozambique Channel Eddies. *Geophysical Research Letters*, *37*, L04604. https://doi.org/10.1029/2009GL041950

Barnier, B., Madec, G., Penduff, T., Molines, J., Treguier, A. M., Le Sommer, J., et al. (2006). Impact of partial steps and momentum advection schemes in a global ocean circulation model at eddy-permitting resolution. *Ocean Dynamics*, *56*(5-6), 543–567. https://doi.org/10.1007/s10236-006-0082-1

Beal, L. M., & Elipot, S. (2016). Broadening not strengthening of the Agulhas Current since the early 1990s. *Nature*, *540*, 570–573. https://doi.org/10.1038/nature19853

Beal, L. M., Elipot, S., Houk, A., & Leber, G. M. (2015). Capturing the transport variability of a western boundary jet: Results from the Agulhas Current Time-Series Experiment (ACT). *Journal of Physical Oceanography*, *45*(5), 1302–1324. https://doi.org/10.1175/JPO-D-14-0119.1

Biastoch, A., Beal, L. M., Lutjeharms, J. R. E., & Casal, T. G. D. (2009). Variability and coherence of the Agulhas Udercurrent in a high-resolution ocean general circulation model. *Journal of Physical Oceanography*, *39*(10), 2417–2435. https://doi.org/10.1175/2009JPO4184.1

Biastoch, A., Durgadoo, J. V., Morrison, A. K., van Sebille, E., Weijer, W., & Griffies, S. M. (2015). Atlantic Multi-decadal oscillation covaries with Agulhas leakage. *Nature Communications*, *6*, 10082. https://doi.org/10.1038/ncomms10082, in prep.

Bleck, R. (2002). An oceanic general circulation model framed in hybrid isopycnic-Cartesian coordinates. *Ocean Modelling*, *4*(1), 55–88. https://doi.org/10.1016/S1463-5003(01)00012-9

Brasnett, B. (2008). The impact of satellite retrievals in a global sea-surface-temperature analysis. *Quarterly Journal of the Royal Meteorological Society*, *1760*(September), 1745–1760. https://doi.org/10.1002/qj

Browning, G. L., & Kreiss, H. O. (1982). Initialization of the shallow water equations with open boundaries by the bounded derivative method. *Tellus*, *34*, 334–351.

Chapman, P., & Largier, J. L. (1989). On the origin of Agulhas Bank bottom water. *South African Journal of Science*, *85*(January), 515–519.

Chelton, D. B., DeSzoeke, R. A., Schlax, M. G., El Naggar, K., & Siwertz, N. (1998). Geographical variability of the first baroclinic Rossby radius of deformation. *Journal of Physical Oceanography*, *28*(3), 433–460. https://doi.org/10.1175/1520-0485(1998)028<0433:GVOTFB>2.0.CO;2

Condie, S. (1995). Interactions between western boundary current and shelf waters: A mechanism for coastal upwelling. *Journal of Geophysical Research*, *100*(C12), 24,811–24,818.

Cronin, M. F., Tozuka, T., Biastoch, A., Durgadoo, J. V., & Beal, L. M. (2013). Prevalence of strong bottom currents in the greater Agulhas system. *Geophysical Research Letters*, *40*, 1772–1776. https://doi.org/10.1002/grl.50400

de Ruijter, W. P. M. D., van Leeuwen, P. J., & Lutjeharms, J. (1999). Generation and evolution of Natal Pulses : Solitary meanders in the Agulhas Current. *Journal of Physical Oceanography*, *29*, 3043–3055.

Debreu, L., & Blayo, E. (2008). Two-way embedding algorithms: A review. *Ocean Dynamics*, *58*(5-6), 415–428. https://doi.org/10.1007/s10236-008-0150-9

Dee, D. P., Uppala, S. M., Simmons, A. J., Berrisford, P., Poli, P., Kobayashi, S., et al. (2011). The ERA-Interim reanalysis: Configuration and performance of the data assimilation system. *Quarterly Journal of the Royal Meteorological Society*, *137*(656), 553–597. https://doi.org/10.1002/qj.828

Durgadoo, J. V., Loveday, B. R., Reason, C. J. C., Penven, P., & Biastoch, A. (2013). Agulhas leakage predominantly responds to the Southern Hemisphere westerlies. *Journal of Physical Oceanography*, *43*(10), 2113–2131. https://doi.org/10.1175/JPO-D-13-047.1

Elipot, S., & Beal, L. M. (2015). Characteristics, energetics, and origins of Agulhas Current meanders and their limited influence on ring shedding. *Journal of Physical Oceanography*, *45*(9), 2294–2314. https://doi.org/10.1175/JPO-D-14-0254.1

George, M. S., Bertino, L., Johannessen, O. M., & Samuelsen, A. (2010). Validation of a hybrid coordinate ocean model for the Indian Ocean. *Journal of Operational Oceanography*, *3*(2), 25–38. https://doi.org/10.1080/1755876X.2010.11020115

Gill, A. E., & Schumann, E. (1979). Topographically induced changes in the structure of an inertial coastal jet: Application to the Agulhas Current. *Journal of Physical Oceanographyhysical Oceanography*, *9*, 975–991.

Halo, I., Backeberg, B., Penven, P., Ansorge, I., Reason, C., & Ullgren, J. (2014). Eddy properties in the Mozambique Channel: A comparison between observations and two numerical ocean circulation models. *Deep Sea Research Part II: Topical Studies in Oceanography*, *100*, 1–16. https://doi.org/10.1016/j.dsr2.2013.10.015

Holton, L., Deshayes, J., Backeberg, B. C., Loveday, B. R., Hermes, J. C., & Reason, C. J. C. (2017). Spatio-temporal characteristics of Agulhas leakage: A model inter-comparison study. *Climate Dynamics*, *48*(7), 1–15. https://doi.org/10.1007/s00382-016-3193-5

Hutchings, L., Beckley, L. E., Griffiths, M. H., Roberts, M. J., Sundby, S., & van der Lingen, C. (2002). Spawning on the edge : Spawning grounds and nursery areas around the southern African coastline. *Marine and Freshwater Research*, *53*, 307–318. https://doi.org/10.1071/MF01147

Krug, M., Swart, S., & Gula, J. (2017). Submesoscale cyclones in the Agulhas Current. *Geophysical Research Letters*, *44*, 346–354. https://doi.org/10.1002/2016GL071006

Krug, M., & Tournadre, J. (2012). Satellite observations of an annual cycle in the Agulhas Current. *Geophysical Research Letters*, *39*, L15607. https://doi.org/10.1029/2012GL052335

Krug, M., Tournadre, J., & Dufois, F. (2014). Interactions between the Agulhas Current and the eastern margin of the Agulhas Bank. *Continental Shelf Research*, *81*, 67–79. https://doi.org/10.1016/j.csr.2014.02.020

Large, W. G., Mcwilliams, J. C., & Doney, S. C. (1994). Oceanic vertical mixing—A review and a model with a nonlocal boundary-layer parameterization. *Reviews of Geophysics*, *32*(94), 363–403. https://doi.org/10.1029/94RG01872

Largier, J. L., & Swart, V. P. (1987). East-west variation in thermocline breakdown on the Agulhas Bank. *South African Journal Of Marine Science*, *5*(1), 263–272.

Le Bars, D., Durgadoo, J. V., Dijkstra, H. A., Biastoch, A., & De Ruijter, W. P. M. (2014). An observed 20-year time series of Agulhas leakage. *Ocean Science*, *10*(4), 601–609. https://doi.org/10.5194/os-10-601-2014

Leber, G. M., & Beal, L. M. (2015). Local water mass modifications by a solitary meander in the Agulhas Current. *Journal of Geophysical Research: Oceans*, *120*, 4503–4515. https://doi.org/10.1002/2015JC010863

Leber, G. M., Beal, L. M., & Elipot, S. (2016). Wind and current forcing combine to drive strong upwelling in the Agulhas Current. *Journal of Physical Oceanography*, pp. JPO–D–16–0079.1. https://doi.org/10.1175/JPO-D-16-0079.1

Loveday, B. R., Durgadoo, J. V., Reason, C. J. C., Biastoch, A., & Penven, P. (2014). Decoupling of the Agulhas Leakage from the Agulhas Current. *Journal of Physical Oceanography*, *44*(7), 1776–1797. https://doi.org/10.1175/JPO-D-13-093.1

Lutjeharms, J. (2006). *The Agulhas Current* (329 pp.). Berlin: Springer.

Lutjeharms, J. R. E., Boebel, O., & Rossby, H. T. (2003). Agulhas cyclones. *Deep-Sea Research Part II: Topical Studies in Oceanography*, *50*(1), 13–34. https://doi.org/10.1016/S0967-0645(02)00378-8

Lutjeharms, J. R. E., Cooper, J., & Roberts, M. (2000). Upwelling at the inshore edge of the Agulhas Current. *Continental Shelf Research*, *20*(7), 737–761. https://doi.org/10.1016/S0278-4343(99)00092-8

Lutjeharms, J. R. E., & Roberts, H. (1988). The Natal Pulse: An extreme transient on the Agulhas Current. *Journal of Geophysical Research*, *93*, 631–645.

MacCready, P., & Rhines, P. B. (1993). Slippery bottom boundary layers on a slope. *Journal of Physical Oceanography*, *23*, 5–22. https://doi.org/10.1175/1520-0485(1993)023<0005:SBBLOA>2.0.CO;2

Madec, G. (2008). NEMO reference manual, ocean dynamic component: NEMO-OPA. Note du 645 Pôle de modélisation (Tech. Rep.). France: Institut Pierre Simon Laplace.

Oki, T., & Sud, Y. C. (1998). Design of Total Runoff Integrating Pathways (TRIP)—A global river channel network. *Earth Interactions*, *2*(1), 1–36. https://doi.org/10.1175/1087-3562(1998)002<0001:DoTRIP>2.0.CO;2

Paldor, N., & Lutjeharms, J. R. E. (2009). Why is the stability of the Agulhas Current geographically bi-modal? *Geophysical Research Letters*, *36*, L14604. https://doi.org/10.1029/2009GL038445

Penven, P., Herbette, S., & Rouault, M. (2011). Ocean modelling in the Agulhas Current System. In *Proc. Nansen-Tutu Conf* (pp. 17–21). Cape Town, South Africa.

Pivan, X., Krug, M., & Herbette, S. (2016). Observations of the vertical and temporal evolution of a Natal Pulse along the Eastern Agulhas Bank. *Journal of Geophysical Research: Oceans*, *121*, 7108–7122. https://doi.org/10.1002/2015JC010796

Quartly, G. D., de Cuevas, B. A., & Coward, A. C. (2013). Mozambique Channel eddies in GCMs: A question of resolution and slippage. *Ocean Modelling*, *63*, 56–67. https://doi.org/10.1016/j.ocemod.2012.12.011

Roberts, M. J. (2005). Chokka squid (Loligo vulgaris reynaudii) abundance linked to changes in 661 South Africa's Agulhas Bank ecosystem during spawning and the early life cycle. *ICES Journal of Marine Science*, *62*, 33–55. https://doi.org/10.1016/j.icesjms.2004.10.002

Roberts, M. J., van der Lingen, C. D., Whittle, C., & van den Berg, M. (2010). Shelf currents, lee-trapped and transient eddies on the inshore boundary of the Agulhas Current, South Africa: Their relevance to the KwaZulu-Natal sardine run. *African Journal of Marine Science*, *32*(2), 423–447. https://doi.org/10.2989/1814232X.2010.512655

Rouault, M. J., & Penven, P. (2011). New perspectives on Natal Pulses from satellite observations. *Journal of Geophysical Research*, *116*, 1–14. https://doi.org/10.1029/2010JC006866

Roughan, M. (2004). On the East Australian Current: Variability, encroachment, and upwelling. *Journal of Geophysical Research*, *109*, C07003. https://doi.org/10.1029/2003JC001833

Roughan, M., & Middleton, J. H. (2002). A comparison of observed upwelling mechanisms off the east coast of Australia. *Continental Shelf Research*, *22*(17), 2551–2572. https://doi.org/10.1016/S0278-4343(02)00101-2

Schaeffer, A., Roughan, M., & Morris, B. D. (2013). Cross-shelf dynamics in a western boundary current regime: Implications for upwelling. *Journal of Physical Oceanography*, *43*(5), 1042–1059. https://doi.org/10.1175/JPO-D-12-0177.1

Schiller, R. V., & Kourafalou, V. H. (2010). Modeling river plume dynamics with the HYbrid Coordinate Ocean Model. *Ocean Modelling*, *33*(1-2), 101–117. https://doi.org/10.1016/j.ocemod.2009.12.005

Schouten, M. W., Ruijter, W. P. M. D., & Leeuwen, P. J. V. (2002). Upstream control of Agulhas Ring shedding. *Journal of Geophysical Research*, *107*(23), 1–12. https://doi.org/10.1029/2001JC000804

Speich, S., Lutjeharms, J. R. E., Penven, P., & Blanke, B. (2006). Role of bathymetry in Agulhas Current configuration and behaviour. *Geophysical Research Letters*, *33*, L23611. https://doi.org/10.1029/2006GL027157

Sutyrin, G. G. (2016). On sharp vorticity gradients in elongating baroclinic eddies and their stabilization with a solid-body rotation. *Geophysical Research Letters*, *43*, 5802–5811. https://doi.org/10.1002/2016GL069019

Swart, V. P., & Largier, J. L. (1987). Thermal structure of Agulhas Bank water. *South African Journal Of Marine Science*, *5*(July 2015), 243–253. https://doi.org/10.2989/025776187784522153

Tsugawa, M., & Hasumi, H. (2010). Generation and growth mechanism of the Natal Pulse. *Journal of Physical Oceanography*, *40*(7), 1597–1612. https://doi.org/10.1175/2010JPO4347.1

van Leeuwen, P. J., de Ruijter, W. P. M., & Lutjeharms, J. R. E. (2000). Natal Pulses and the formation of Agulhas rings. *Journal of Geophysical Research*, *105*, 6425–6436. https://doi.org/10.1029/1999JC900196